Soft-lubrication interactions between a rigid sphere and an elastic wall

Vincent Bertin,[1,2] Yacine Amarouchene,[1] Elie Raphaël,[2] and Thomas Salez[1,3,*]

[1]*Univ. Bordeaux, CNRS, LOMA, UMR 5798, 33405 Talence, France.*

[2]*UMR CNRS Gulliver 7083, ESPCI Paris, PSL Research University, 75005 Paris, France.*

[3]*Global Station for Soft Matter, Global Institution for Collaborative Research and Education, Hokkaido University, Sapporo, Hokkaido 060-0808, Japan.*

(Dated:)

The motion of an object within a viscous fluid and in the vicinity of a soft surface induces a hydrodynamic stress field that deforms the latter, thus modifying the boundary conditions of the flow. This results in elastohydrodynamic (EHD) interactions experienced by the particle. Here, we derive a soft-lubrication model, in order to compute all the forces and torque applied on a rigid sphere that is free to translate and rotate near an elastic wall. We focus on the limit of small deformations of the surface with respect to the fluid-gap thickness, and perform a perturbation analysis at leading order in dimensionless compliance. The response is computed in the limiting cases of thick and thin elastic materials. The normal force is also obtained analytically using the Lorentz reciprocal theorem and agrees with the numerical results.

INTRODUCTION

The fluid-structure interaction between flows and boundaries is a central situation in continuum mechanics, encountered at many length and velocity scales. A classical example is lubrication, where the addition of a liquid film, a lubricant, between two contacting objects, allows for a drastic reduction of the friction between them. Such a process occurs in a large variety of contexts with hard materials, such as roller bearings, pistons and gears in industry [1], or faults [2] and landslides [3] in geological settings. At large velocity, or moderate loading, the liquid film is continuous with no direct contact between the solids. When the solids are deformable, the friction force can be described using elastohydrodynamic (EHD) models within the soft-lubrication approximation [1].

The previous EHD coupling is also widely encountered in soft condensed matter, but at very different pressure and velocity scales [4]. Examples encompass the remarkable frictional properties of eyelids [5] and cartilaginous joints [6, 7], as well as biomimetic gels [8] and rubbers [9–12]. Of interest as well are the collisions and rebounds of spheres in viscous environments [13–15], the rheological properties of soft suspensions and pastes [9, 16], and the self-similar properties of the contact [17].

In the last decade, EHD interactions have been of great interest in the material-science community with the emergence of contactless rheological methods to measure the mechanical properties of confined liquids and soft surfaces [18–29]. Typically, in such experimental systems, a spherical colloidal probe is immersed in a fluid and driven to oscillate, with a nanometric amplitude, near a surface of interest. The force exerted on the probe is measured by an atomic force microscope, a surface force apparatus or a tuning-fork microscope, and depends on the properties of both the fluid and the solid boundary.

Generally, an object that moves in a confined fluid environment experiences an enhanced drag force with respect to the bulk Stokes law, as a result of the boundary-induced flow modification [30]. Furthermore, near a soft wall, the hydrodynamic interactions are modified by the deformation of the boundary that they generate, yielding a nonlinear coupling. Perturbation methods, assuming a small deformation of the interface, have been employed in order to calculate the soft-lubrication interactions exerted on a free infinite cylinder immersed in a viscous fluid and near a thin compressible elastic material [31]. In particular, interesting inertial-like features have been predicted despite the low-Re-number aspect of the flow.

Perhaps the most emblematic example of soft-lubrication interaction is the non-inertial lift force predicted for a particle sliding near a soft boundary [9, 32–36]. It might have important implications for advected biological entities, such as red blood cells [37] and vesicles [38]. Only recently, the associated dynamical repulsion from an immersed soft interface has been studied experimentally. A preliminary qualitative observation was reported in the context of smart lubricants and elastic polyelectrolytes [39]. Then, a study involving the sliding of an immersed macroscopic cylinder along an inclined plane pre-coated with a thin layer of gel, showed quantitatively an effective reduction of friction induced by the EHD lift force [40]. Subsequently, the same effect was observed in the trajectories of micrometric spherical beads within a microfluidic channel coated with a biomimetic polymer layer [41], and through the sedimentation of a macroscopic sphere near a pre-tensed suspended elastic membrane [42]. Finally, direct measurements of the EHD lift force for two types of elastic materials have been performed at small scales, using surface force apparatus and atomic force microscopy, respectively [43, 44].

Despite the increasing number of EHD studies involving spherical probes, the soft-lubrication interactions of a free spherical object immersed in a viscous fluid and moving near an elastic substrate still have to be calculated. In the present article, we aim at filling this gap by deriving a soft-lubrication perturbation theory, in order to compute all the forces and torque for this problem, at leading order in dimensionless compliance.

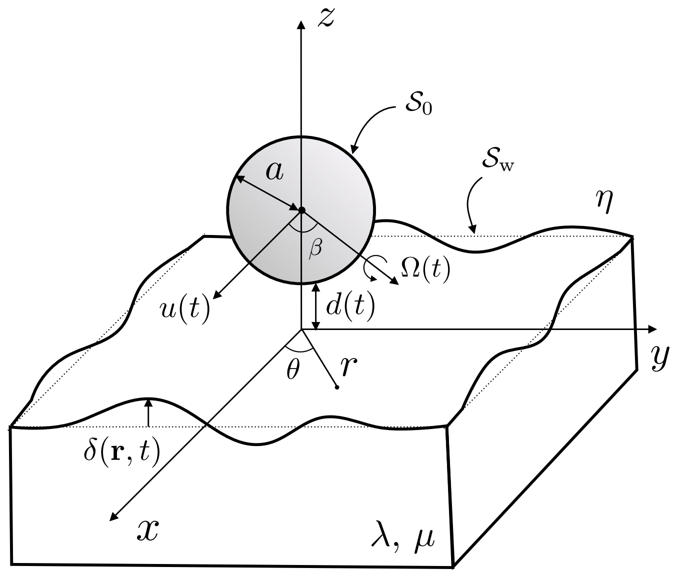

Figure 1: Schematic of the system. A rigid sphere of surface $\mathcal{S}_0$ is freely moving in a viscous fluid, near a soft wall of surface $\mathcal{S}_\mathrm{w}$ in the undeformed state. The lubrication pressure field deforms the latter which induces an elastohydrodynamic coupling, with forces and torque exerted on the sphere.

The article is organized as follows. In section , we introduce the soft-lubrication framework for a sphere translating near a soft planar surface, both in the normal and tangential directions. The substrate deformation is assumed to follow the constitutive response of a linear elastic semi-infinite material. In section , we perform a perturbative approach, assuming the substrate deformation to be small with respect to the fluid-gap thickness, which allows us to find the normal and tangential forces as well as the torque experienced by the sphere, at leading order in dimensionless compliance. In section , we discuss the rotation of the sphere. Concluding remarks are given in section . Besides, the normal EHD force is computed analytically in appendix , using the Lorentz reciprocal theorem, while the procedure introduced in section is reproduced for the compressible and incompressible responses of a thin material in appendixes and , respectively.

MODEL

The system is depicted in Fig. 1. We consider a sphere of radius a, neutrally-buoyant within a Newtonian fluid of dynamic shear viscosity η and density ρ. The sphere is moving with a tangential velocity $\boldsymbol{u}(t) = u(t)\,\boldsymbol{e}_x$ directed along the x-axis (by definition of the latter axis), where $\boldsymbol{e}_j$ denotes the unit vector along j. In this first part, we assume that the sphere does not rotate, *i.e.* the angular velocity reads $\boldsymbol{\Omega} = \boldsymbol{0}$. The sphere is placed at a time-dependent distance $d(t)$ (thus a $\dot{d}\,\boldsymbol{e}_z$ vertical velocity of the sphere) of an elastic substrate of Lamé coefficients λ and μ, with a reference undeformed flat surface in the xy plan at $z = 0$. The Reynolds number $\mathrm{Re} = \rho u a/\eta$ is assumed to be small with respect to unity such that the velocity and pressure fields, $\boldsymbol{v}$ and p respectively, follow the Stokes equations. In addition, we place ourselves in the steady incompressible case, and further suppose that the sphere-wall distance is small with respect to the sphere radius, such that the lubrication approximation is valid. No-slip boundary conditions are assumed at both the sphere and wall surfaces. Finally, the system is equivalent to a sphere at rest near a wall translating with a $-\boldsymbol{u}(t)$ velocity. In such a framework, the fluid velocity field can be written as:

$$\boldsymbol{v}(\boldsymbol{r},z,t) = \frac{\boldsymbol{\nabla}p(\boldsymbol{r},t)}{2\eta}(z-h_0(r,t))(z-\delta(\boldsymbol{r},t)) - \boldsymbol{u}(t)\frac{h_0(r,t)-z}{h_0(r,t)-\delta(\boldsymbol{r},t)}, \tag{1}$$

where $\boldsymbol{r} = (r,\theta)$ is the position in the tangential plane xy, $\boldsymbol{\nabla}$ is the 2D gradient operator on xy, $\delta(\boldsymbol{r},t)$ is the substrate deformation, and $z = h_0(r,t)$ is the sphere surface. Near contact, the latter can be approximated by its parabolic expansion $h_0(r,t) \simeq d(t) + r^2/(2a)$. Volume conservation further leads to the Reynolds equation:

$$\partial_t h(\boldsymbol{r},t) = \boldsymbol{\nabla}\cdot\left(\frac{h^3(\boldsymbol{r},t)}{12\eta}\boldsymbol{\nabla}p(\boldsymbol{r},t) + \frac{h(\boldsymbol{r},t)}{2}\boldsymbol{u}(t)\right), \tag{2}$$

where $h(\boldsymbol{r},t) = h_0(r,t) - \delta(\boldsymbol{r},t)$ is the fluid-gap thickness. In this first part, we assume that the constitutive elastic response is linear and instantaneous, and that the substrate is a semi-infinite medium, such that the deformation reads:

$$\delta(\boldsymbol{r},t) = -\frac{(\lambda+2\mu)}{4\pi\mu(\lambda+\mu)}\int_{\mathbb{R}^2} \mathrm{d}^2\boldsymbol{x}\,\frac{p(\boldsymbol{x},t)}{|\boldsymbol{r}-\boldsymbol{x}|}. \tag{3}$$

We non-dimensionalize the problem through:

$$h(\boldsymbol{r},t) = d^*H(\boldsymbol{R},T), \quad \boldsymbol{r} = \sqrt{2ad^*}\,\boldsymbol{R}, \quad d(t) = d^*D(T), \quad \delta(\boldsymbol{r},t) = d^*\Delta(\boldsymbol{R},T), \tag{4}$$

$$p(\boldsymbol{r},t) = \frac{\eta c\sqrt{2ad^*}}{d^{*2}}\,P(\boldsymbol{R},T), \quad \boldsymbol{u}(t) = c\,U(T)\,\boldsymbol{e}_x, \quad \boldsymbol{v} = c\boldsymbol{V}, \quad t = \frac{\sqrt{2ad^*}}{c}\,T. \tag{5}$$

where d^* and c are characteristic fluid-gap distance and lateral velocity, respectively. The governing equations are then:

$$12\partial_T H(\boldsymbol{R},T) = \boldsymbol{\nabla}\cdot\Big(H^3(\boldsymbol{R},T)\boldsymbol{\nabla}P(\boldsymbol{R},T) + 6H(\boldsymbol{R},T)\boldsymbol{U}(T)\Big), \tag{6}$$

$$H(\boldsymbol{R},T) = D(T) + R^2 - \Delta(\boldsymbol{R},T), \tag{7}$$

and:

$$\Delta(\boldsymbol{R},T) = -\kappa\int_{\mathbb{R}^2} \mathrm{d}^2\boldsymbol{X}\,\frac{P(\boldsymbol{X},T)}{4\pi|\boldsymbol{R}-\boldsymbol{X}|}, \tag{8}$$

where we introduced the dimensionless compliance:

$$\kappa = \frac{2\eta ca(\lambda+2\mu)}{d^{*2}\mu(\lambda+\mu)}. \tag{9}$$

The latter is the only dimensionless parameter in the problem. When κ is small with respect to unity, it corresponds to the ratio between two length scales: the typical substrate deformation $\delta \sim \frac{2\eta ca(\lambda+2\mu)}{d^*\mu(\lambda+\mu)}$ induced by a lateral velocity c, and the typical fluid-gap thickness d^*. All along the article, we focus on the small-deformation regime of soft-lubrication where $\kappa \ll 1$ [45].

PERTURBATION THEORY

We perform a perturbation analysis at small κ [9, 31–36, 44, 46–48], as follows:

$$H(\boldsymbol{R},T) = H_0(\boldsymbol{R},T) + \kappa\,H_1(\boldsymbol{R},T) + O(\kappa^2), \tag{10}$$

$$P(\boldsymbol{R},T) = P_0(\boldsymbol{R},T) + \kappa\,P_1(\boldsymbol{R},T) + O(\kappa^2), \tag{11}$$

where the subscript 0 corresponds to the solution for a rigid wall, with $H_0(\boldsymbol{R},T) = D(T) + R^2$.

Leading-order solution

Equation (6) reads at zeroth order $O(\kappa^0)$:

$$12\dot{D} = \boldsymbol{\nabla}\cdot\Big(H_0^3\boldsymbol{\nabla}P_0 + 6H_0\boldsymbol{U}\Big). \tag{12}$$

In polar coordinates, Eq. (12) can be rewritten as:

$$\mathcal{L}.P_0 = R^2\partial_R^2 P_0 + \left(R + \frac{6R^3}{D+R^2}\right)\partial_R P_0 + \partial_\theta^2 P_0 = \frac{R^2}{(D+R^2)^3}\Big(12\dot{D} - 12R\cos\theta\,U\Big), \tag{13}$$

where $\mathcal{L}$ is a linear operator. We solve this equation, using an angular-mode decomposition:

$$P_0(\boldsymbol{R},T) = P_0^{(0)}(R,T) + P_0^{(1)}(R,T)\cos\theta, \tag{14}$$

where the two coefficients are solutions of the ordinary differential equations:

$$R^2\frac{\mathrm{d}^2P_0^{(0)}}{\mathrm{d}R^2} + \left(R + \frac{6R^3}{D+R^2}\right)\frac{\mathrm{d}P_0^{(0)}}{\mathrm{d}R} = 12\frac{R^2\dot{D}}{(D+R^2)^3}, \tag{15a}$$

$$R^2\frac{\mathrm{d}^2P_0^{(1)}}{\mathrm{d}R^2} + \left(R + \frac{6R^3}{D+R^2}\right)\frac{\mathrm{d}P_0^{(1)}}{\mathrm{d}R} - P_0^{(1)} = -12\frac{R^3U}{(D+R^2)^3}. \tag{16a}$$

In accordance with the boundary conditions, $P(R\to\infty)=0$ and $P(R=0)<\infty$, the solution is thus:

$$P_0(\boldsymbol{R},T) = -\frac{3\dot{D}}{2(D+R^2)^2} + \frac{6RU\cos\theta}{5(D+R^2)^2}. \tag{17}$$

The leading-order substrate deformation H_1 can then be computed from Eq. (8) at order $O(\kappa)$:

$$H_1(\boldsymbol{R},T) = \int_{\mathbb{R}^2}\mathrm{d}^2\boldsymbol{X}\,\frac{P_0(\boldsymbol{X},T)}{4\pi|\boldsymbol{R}-\boldsymbol{X}|}. \tag{18}$$

Using *e.g.* the spatial Fourier transform $\tilde{H}_1(\boldsymbol{K}) = \int_{\mathbb{R}^2} H_1(\boldsymbol{R})e^{-i\boldsymbol{R}.\boldsymbol{K}}\mathrm{d}^2\boldsymbol{R}$, we find:

$$H_1(\boldsymbol{R},T) = -\frac{3\dot{D}}{8\sqrt{D}}\,\frac{\mathcal{E}(-R^2/D)}{D+R^2} + \frac{3U}{10R\sqrt{D}}\left(-\frac{D\,\mathcal{E}(-R^2/D)}{D+R^2} + \mathcal{K}(-R^2/D)\right)\cos\theta, \tag{19}$$

where $\mathcal{K}$ and $\mathcal{E}$ are complete elliptic integrals of the first and second kinds [49].

Next-order solution

We can now compute the next-order pressure field P_1, from Eq. (6) at order $O(\kappa)$:

$$12\partial_T H_1 = \boldsymbol{\nabla}\cdot\left(H_0^3\boldsymbol{\nabla}P_1 + 3H_0^2H_1\boldsymbol{\nabla}P_0 + 6H_1\boldsymbol{U}\right). \tag{20}$$

Invoking the same linear operator $\mathcal{L}$ as in Eq. (13), we can rewrite Eq. (20) as:

$$\mathcal{L}.P_1 = \frac{R^2}{H_0^3}\left(12\partial_T H_1 - \boldsymbol{\nabla}\cdot\left[3H_0^2H_1\boldsymbol{\nabla}P_0 + 6H_1\boldsymbol{U}\right]\right). \tag{21}$$

We then expand all the terms in the right-hand side of Eq. (21), and we perform once again the angular-mode decomposition:

$$\mathcal{L}.P_1 = F_0(R,T) + F_1(R,T)\cos\theta + F_2(R,T)\cos 2\theta, \tag{22}$$

where we have introduced the auxiliary functions:

$$\begin{aligned}F_0(R,T) = {}& \frac{18R^2U^2}{25D^{1/2}(D+R^2)^6}\left[(-10D^2+2DR^2)\,\mathcal{E}\left(-\frac{R^2}{D}\right) + (8D^2+7DR^2-R^4)\,\mathcal{K}\left(-\frac{R^2}{D}\right)\right] \\ &+ \frac{9R^2\dot{D}^2}{4D^{3/2}(D+R^2)^6}\left[(13D^2+3R^2D+2R^4)\,\mathcal{E}\left(-\frac{R^2}{D}\right) + (-4D^2-5R^2D-R^4)\,\mathcal{K}\left(-\frac{R^2}{D}\right)\right] \\ &- \frac{9R^2\ddot{D}\,\mathcal{E}\left(-\frac{R^2}{D}\right)}{2D^{1/2}(D+R^2)^4},\end{aligned} \tag{23}$$

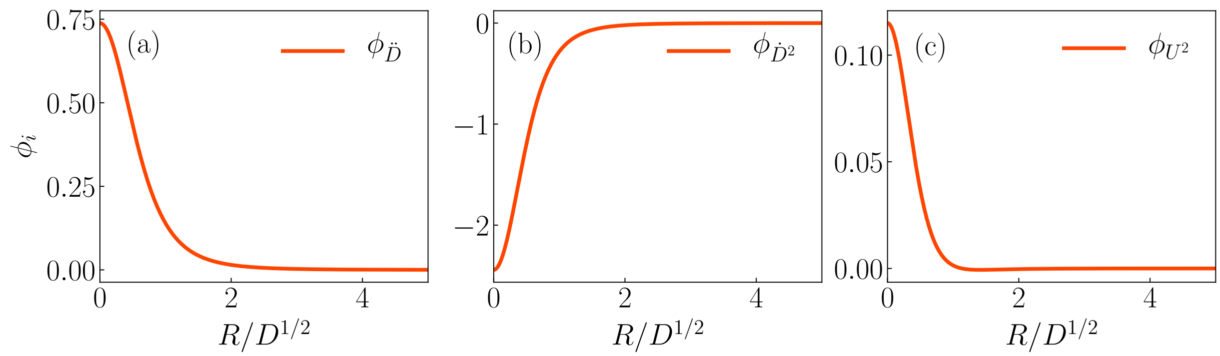

Figure 2: Scaling functions for $P_1^{(0)}$ (see Eq. (27)), obtained from numerical integration of Eq. (25), with the boundary conditions $\partial_R P_1^{(0)}(R=0,T)=0$ and $P_1^{(0)}(R\to\infty,T)=0$.

and:

$$F_1(R,T) = -\frac{27RU\dot{D}}{5D^{1/2}(D+R^2)^6}\left[(-2D^2+7DR^2+R^4)\,\mathcal{E}\left(-\frac{R^2}{D}\right)+2(D+R^2)(D-R^2)\,\mathcal{K}\left(-\frac{R^2}{D}\right)\right]$$
$$-\frac{18R\dot{U}}{5D^{1/2}(D+R^2)^4}\left[-D\,\mathcal{E}\left(-\frac{R^2}{D}\right)+(D+R^2)\,\mathcal{K}\left(-\frac{R^2}{D}\right)\right]. \tag{24}$$

We note that we have not provided F_2 as it does not contribute in the forces and torque. We also note that, by setting $D(T)=1$ in the latter expressions, we self-consistently recover the expression of [44]. Invoking the angular-mode decomposition $P_1(\boldsymbol{R},T)=P_1^{(0)}(R,T)+P_1^{(1)}(R,T)\cos\theta+P_1^{(2)}(R,T)\cos 2\theta$, we get in particular:

$$R^2\frac{\mathrm{d}^2P_1^{(0)}}{\mathrm{d}R^2}+\left(R+\frac{6R^3}{D+R^2}\right)\frac{\mathrm{d}P_1^{(0)}}{\mathrm{d}R}=F_0(R,T), \tag{25}$$

$$R^2\frac{\mathrm{d}^2P_1^{(1)}}{\mathrm{d}R^2}+\left(R+\frac{6R^3}{D+R^2}\right)\frac{\mathrm{d}P_1^{(1)}}{\mathrm{d}R}-P_1^{(1)}=F_1(R,T). \tag{26}$$

Using scaling arguments, we can write the two relevant next-order pressure components $P_1^{(i)}$ as:

$$P_1^{(0)}=\frac{U^2}{D^{7/2}}\phi_{U^2}(R/\sqrt{D})+\frac{\dot{D}^2}{D^{9/2}}\phi_{\dot{D}^2}(R/\sqrt{D})+\frac{\ddot{D}}{D^{7/2}}\phi_{\ddot{D}}(R/\sqrt{D}), \tag{27}$$

and:

$$P_1^{(1)}=\frac{U\dot{D}}{D^4}\phi_{U\dot{D}}(R/\sqrt{D})+\frac{\dot{U}}{D^3}\phi_{\dot{U}}(R/\sqrt{D}), \tag{28}$$

where the ϕ_i are five dimensionless scaling functions that depend on the self-similar variable $R/\sqrt{D}$ only. Equations (27) and (28) can be solved numerically with a Runge-Kutta algorithm, and a shooting parameter in order to ensure the boundary condition $P_1(R\to\infty,\theta,T)=0$. All the scaling functions are plotted in Figs. 2 and 3.

Forces and torque

The force $\boldsymbol{F}$ exerted by the fluid on the sphere is given by:

$$\boldsymbol{F}=\int_{\mathcal{S}_0}\boldsymbol{n}\cdot\boldsymbol{\sigma}\,\mathrm{d}s, \tag{29}$$

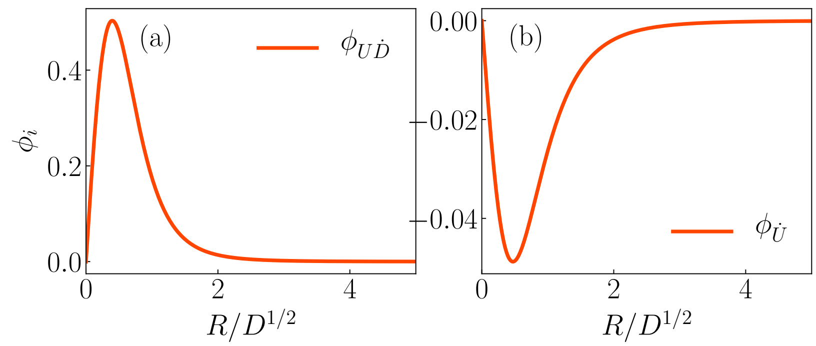

Figure 3: Scaling functions for $P_1^{(1)}$ (see Eq. (28)), obtained from numerical integration of Eq. (26), with the boundary conditions $P_1^{(1)}(R = 0, T) = 0$ and $P_1^{(1)}(R \to \infty, T) = 0$.

where $\boldsymbol{\sigma} = -p\mathbf{I} + \eta(\boldsymbol{\nabla v} + \boldsymbol{\nabla v}^{\mathrm{T}})$ is the fluid stress tensor, $\boldsymbol{n}$ is the unit vector normal to the sphere surface and pointing towards the fluid, and $\mathbf{I}$ is the identity tensor. Within the lubrication approximation, the leading-order fluid stress tensor reads $\boldsymbol{\sigma} \simeq -p\mathbf{I} + \eta \boldsymbol{e}_z \partial_z \boldsymbol{v}$. One can then evaluate the vertical force, at leading order in the lubrication parameter $\frac{d}{a}$, as:

$$F_z = \int_{\mathbb{R}^2} p(\boldsymbol{r})\,\mathrm{d}^2\boldsymbol{r} = -\frac{6\pi\eta a^2 \dot{d}}{d} + 0.416\frac{\eta^2 u^2(\lambda+2\mu)}{\mu(\lambda+\mu)}\left(\frac{a}{d}\right)^{5/2} - 41.91\frac{\eta^2 \dot{d}^2(\lambda+2\mu)}{\mu(\lambda+\mu)}\left(\frac{a}{d}\right)^{7/2} + 18.49\frac{\eta^2 \ddot{d} a(\lambda+2\mu)}{\mu(\lambda+\mu)}\left(\frac{a}{d}\right)^{5/2}, \tag{30}$$

where the prefactors have been found numerically using Eq. (27). In appendix , following previous works [42, 47, 50, 51], we use the Lorentz reciprocal theorem in order to recover the prefactors of Eq. (30) analytically, which gives respectively: $\frac{243\pi^3}{12800\sqrt{2}} \approx 0.416$, $\frac{3915\pi^3}{2048\sqrt{2}} \approx 41.91$ and $\frac{27\pi^3}{32\sqrt{2}} \approx 18.49$. We note that the latter is in agreement with the result of the linear-response theory derived in [20]. Furthermore, we recover the lift prefactor (0.416) obtained previously numerically [44], as well as analytically in a recently-published work [52].

Similarly, at leading order in the lubrication parameter d/a, the tangential force reads:

$$\boldsymbol{F}_\parallel = \int_{\mathbb{R}^2} \left(-p(\boldsymbol{r},t)\frac{\boldsymbol{r}}{a} - \eta\partial_z \boldsymbol{v}\right)_{z=h_0(r,t)} \mathrm{d}^2\boldsymbol{r}. \tag{31}$$

Using symmetry arguments, we can show that the tangential force is directed along x, *i.e.* $\boldsymbol{F}_\parallel = F_x\,\boldsymbol{e}_x$. At small κ, we further expand it as $F_x \simeq F_{x,0} + \kappa F_{x,1}$, where $F_{x,0}$ is the viscous drag force applied on a sphere near a rigid plane wall, and $\kappa F_{x,1}$ is the leading-order EHD correction. The zeroth-order term cannot be evaluated using the lubrication model introduced in the previous section, because the integral in Eq. (31) diverges, as the shear term $\eta\partial_z\boldsymbol{v}$ scales as $\sim r^{-2}$ at large r. An exact calculation has been performed using bispherical coordinates and provides a solution in the form of a series expansion [53]. Asymptotic-matching methods have also been employed in order to get the asymptotic behavior at small d/a [54, 55], which reads $F_{x,0} \approx 6\pi\eta a u\left(\frac{8}{15}\log\left(\frac{d}{a}\right) - 0.95429\right)$. Nevertheless, the leading-order EHD correction can be computed with the present model, as the correction pressure field and shear stress scale as $\sim r^{-5}$, at large r. It reads:

$$F_{x,1} = 2\pi\eta c a \int_0^\infty \left[-2RP_1^{(1)} + \frac{H_0}{2}\left(\partial_R P_1^{(1)} + \frac{P_1^{(1)}}{R}\right) + \frac{H_1^{(1)}}{2}\partial_R P_0^{(0)} + \frac{H_1^{(0)}}{2}\left(\partial_R P_0^{(1)} + \frac{P_0^{(1)}}{R}\right) + 2\frac{UH_1^{(0)}}{H_0^2}\right] R\,\mathrm{d}R. \tag{32}$$

Evaluating the latter integral numerically, we find:

$$F_x \approx 6\pi\eta a u\left(\frac{8}{15}\log\left(\frac{d}{a}\right) - 0.95429\right) - 20.3\frac{\eta^2 u\dot{d}(\lambda+2\mu)}{\mu(\lambda+\mu)}\left(\frac{a}{d}\right)^{5/2} + 2.95\frac{\eta^2 \dot{u} a(\lambda+2\mu)}{\mu(\lambda+\mu)}\left(\frac{a}{d}\right)^{3/2}. \tag{33}$$

The torque exerted by the fluid on the sphere, with respect to its center of mass, is given by:

$$\boldsymbol{T} = \int_{S_0} a\boldsymbol{n} \times (\boldsymbol{n} \cdot \boldsymbol{\sigma})\, \mathrm{d}s. \tag{34}$$

The latter is directed along the y direction for symmetry reasons, *i.e.* $\boldsymbol{T} = T_y\,\boldsymbol{e}_y$. At small κ, we further expand it as $T_y \simeq T_{y,0} + \kappa T_{y,1}$. For the same reason as with the the viscous drag force near a rigid wall, the viscous torque near a rigid wall cannot be computed within the lubrication model. Using asymptotic-matching methods [54], it is found to be $T_{y,0} \approx 8\pi\eta u a^2\left(-\frac{2}{10}\log\left(\frac{d}{a}\right) - 0.19296\right)$. However, the leading-order EHD correction can be computed with the present model, and reads:

$$T_{y,1} = -2\eta c a^2 \pi \int_0^\infty \left[\frac{H_0}{2}\left(\partial_R P_1^{(1)} + \frac{P_1^{(1)}}{R}\right) + \frac{H_1^{(1)}}{2}\partial_R P_0^{(0)} + \frac{H_1^{(0)}}{2}\left(\partial_R P_0^{(1)} + \frac{P_0^{(1)}}{R}\right) + 2\frac{UH_1^{(0)}}{H_0^2}\right] R\, \mathrm{d}R. \tag{35}$$

Evaluating the latter integral numerically, we find:

$$T_y \approx 8\pi\eta u a^2\left(-\frac{1}{10}\log\left(\frac{d}{a}\right) - 0.19296\right) + 10.9\frac{\eta^2 u a \dot{d}(\lambda+2\mu)}{\mu(\lambda+\mu)}\left(\frac{a}{d}\right)^{5/2} - 0.987\frac{\eta^2 \dot{u} a^2(\lambda+2\mu)}{\mu(\lambda+\mu)}\left(\frac{a}{d}\right)^{3/2}. \tag{36}$$

So far, we focused on the particular case of a semi-infinite elastic material. In appendices and , we apply the same soft-lubrication approach to other elastic models describing thin substrates, which are also widespread in practice. We find similar expressions, but with different numerical prefactors and scalings with the sphere-wall distance.

ROTATION

We now add the rotation of the sphere, with angular velocity $\boldsymbol{\Omega}(t)$ in the xy plane (see Fig. 1), to the previous translational motion. We define β as the angle between $\boldsymbol{\Omega}$ and the x-axis. We stress that $\boldsymbol{\Omega}$ is not necessarily orthogonal (*i.e.* $\beta = \pi/2$) to the translation velocity. We discard the rotation along the z-axis (*e.g.* for a spinner), because it does not induce any soft-lubrication coupling. Finally, the system is equivalent to a purely rotating sphere with angular velocity $\boldsymbol{\Omega}(t)$, near a wall translating with a $-\boldsymbol{u}(t)$ velocity. In such a framework, the fluid velocity field at the sphere surface is $\boldsymbol{v} = \boldsymbol{\Omega} \times a\boldsymbol{n}$, and thus $\boldsymbol{v} \simeq \boldsymbol{\Omega} \times a\boldsymbol{e}_z$ at leading-order in the lubrication zone. All together, the fluid velocity field is modified as:

$$\boldsymbol{v}(\boldsymbol{r}, z, t) = \frac{\boldsymbol{\nabla} p(\boldsymbol{r}, t)}{2\eta}(z - h_0(r,t))(z - \delta(\boldsymbol{r}, t)) - \boldsymbol{u}(t)\frac{h_0(r,t) - z}{h_0(r,t) - \delta(\boldsymbol{r},t)} + a\boldsymbol{\Omega}(t) \times \boldsymbol{e}_z\,\frac{z - \delta(\boldsymbol{r},t)}{h_0(r,t) - \delta(\boldsymbol{r},t)}, \tag{37}$$

and the Reynolds equation becomes:

$$\partial_t h(\boldsymbol{r}, t) = \boldsymbol{\nabla}.\left(\frac{h^3(\boldsymbol{r},t)}{12\eta}\boldsymbol{\nabla} p(\boldsymbol{r},t) + \frac{h(\boldsymbol{r},t)}{2}\left[\underbrace{\boldsymbol{u}(t) - a\boldsymbol{\Omega}(t) \times \boldsymbol{e}_z}_{\tilde{\boldsymbol{u}}}\right]\right). \tag{38}$$

The problem is thus formally equivalent to the one of a sphere that is purely translating with effective velocity $\tilde{\boldsymbol{u}}(t) = \boldsymbol{u}(t) - a\boldsymbol{\Omega}(t) \times \boldsymbol{e}_z$. Therefore, we can directly apply the results from the previous sections, and write all the forces and torque exerted on the sphere, as:

$$F_z = -\frac{6\pi\eta a^2 \dot{d}}{d} + 0.416\frac{\eta^2|\boldsymbol{u} - a\boldsymbol{\Omega} \times \boldsymbol{e}_z|^2}{\mu}\left(\frac{a}{d}\right)^{5/2} - 41.91\frac{\eta^2\dot{d}^2}{\mu}\left(\frac{a}{d}\right)^{7/2} + 18.49\frac{\eta^2\ddot{d}a}{\mu}\left(\frac{a}{d}\right)^{5/2}, \tag{39}$$

$$\begin{aligned}\boldsymbol{F}_\parallel = {} & 6\pi\eta a\boldsymbol{u}\left[\frac{8}{15}\log\left(\frac{d}{a}\right) - 0.95429\right] + 6\pi\eta a^2\boldsymbol{e}_z \times \boldsymbol{\Omega}\left[\frac{2}{15}\log\left(\frac{d}{a}\right) + 0.25725\right] \\ & - 20.3\frac{\eta^2(\boldsymbol{u} - a\boldsymbol{\Omega} \times \boldsymbol{e}_z)\dot{d}}{\mu}\left(\frac{a}{d}\right)^{5/2} + 2.95\frac{\eta^2(\dot{\boldsymbol{u}} - a\dot{\boldsymbol{\Omega}} \times \boldsymbol{e}_z)a}{\mu}\left(\frac{a}{d}\right)^{3/2},\end{aligned} \tag{40}$$

and:

$$\boldsymbol{T}_{\parallel} = 8\pi\eta a^2 \boldsymbol{e}_z \times \boldsymbol{u}\left[-\frac{1}{10}\log\left(\frac{d}{a}\right) - 0.19296\right] + 8\pi\eta a^3 \boldsymbol{\Omega}\left[\frac{2}{5}\log\left(\frac{d}{a}\right) - 0.37085\right] \\ + 10.9\frac{\eta^2(\boldsymbol{u} - a\boldsymbol{\Omega}\times\boldsymbol{e}_z)a\dot{d}}{\mu}\left(\frac{a}{d}\right)^{5/2} - 0.987\frac{\eta^2(\dot{\boldsymbol{u}} - a\dot{\boldsymbol{\Omega}}\times\boldsymbol{e}_z)a^2}{\mu}\left(\frac{a}{d}\right)^{3/2}, \tag{41}$$

where we have invoked the force and torque induced by the rotation of a sphere near a rigid wall [36, 55]. We stress that the expressions of the EHD forces and torque for a sphere purely translating near thin elastic substrates, as derived in appendices and , can be generalized to further include the sphere's rotation by similarly following the transformation $\boldsymbol{u}(t) \to \boldsymbol{u}(t) - a\boldsymbol{\Omega}(t)\times\boldsymbol{e}_z$.

CONCLUSION

We developed a soft-lubrication model in order to compute the EHD interactions exerted on an immersed sphere undergoing both translational and rotational motions near various types of elastic walls. The deformation of the surface was assumed to be small, which allowed us to employ a perturbation analysis in order to obtain the leading-order EHD forces and torque. The obtained interaction matrix exhibits a qualitatively similar form as the one found for a two-dimensional cylinder moving near a thin compressible substrate [31]. In both cases, the EHD coupling is nonlinear and generates quadratic terms in the sphere velocity, thus breaking the time-reversal symmetry of the Stokes equations. In addition, linear terms proportional to the acceleration of the sphere are found. Therefore, while the quantitative details such as numerical prefactors and exponents differ in 3D and when using more realistic constitutive elastic responses, we expect that the typical zoology of trajectories identified previously [31] will also hold for spherical objects – and will even be extended with the added degree of freedom. As such, the asymptotic predictions obtained here may open new perspectives in colloidal science and biophysics, through the understanding and control of the emerging interactions within soft confinement or assemblies.

Acknowledgments

We thank Abelhamid Maali and Zaicheng Zhang for stimulating discussions.

Fundings

The authors acknowledge funding from the ANR T-ERC *EMetBrown* and from the Jean Langlois foundation.

Declaration of Interests

The authors report no conflict of interest.

Lorentz reciprocal theorem

In this appendix, we compute the leading-order vertical EHD forces using the Lorentz reciprocal theorem for Stokes flows [42, 47, 50, 51], in order to recover analytically some of the numerical prefactors obtained in section . To do so, we introduce the model problem of a sphere moving in a viscous fluid and towards an immobile, rigid, planar surface. We note $\hat{\boldsymbol{V}} = -\hat{V}\boldsymbol{e}_z$ the velocity at the particle surface $\mathcal{S}_0$, and we assume a no-slip boundary condition at the undeformed wall surface $\mathcal{S}_{\mathrm{w}}$ located at $z = 0$ (see Fig. 1). The viscous stress and velocity fields of the model problem follow the steady, incompressible Stokes equations $\boldsymbol{\nabla}\cdot\hat{\boldsymbol{\sigma}} = \boldsymbol{0}$ and $\boldsymbol{\nabla}\cdot\hat{\boldsymbol{v}} = 0$, and we use the lubrication approximation. In this framework, the stress tensor is $\hat{\boldsymbol{\sigma}} \simeq -\hat{p}\mathbf{I} + \eta\boldsymbol{e}_z\partial_z\hat{\boldsymbol{v}}$, with:

$$\hat{p}(\boldsymbol{r}) = \frac{3\eta\hat{V}a}{\hat{h}^2(\boldsymbol{r})}, \qquad \hat{\boldsymbol{v}}(\boldsymbol{r}, z) = \frac{\boldsymbol{\nabla}\hat{p}(\boldsymbol{r})}{2\eta}z(z - \hat{h}(\boldsymbol{r})), \qquad \hat{h}(\boldsymbol{r}) = d + \frac{\boldsymbol{r}^2}{2a}. \tag{42}$$

The Lorentz reciprocal theorem states that:

$$\int_{\mathcal{S}} \boldsymbol{n} \cdot \boldsymbol{\sigma} \cdot \hat{\boldsymbol{v}} \, \mathrm{d}s = \int_{\mathcal{S}} \boldsymbol{n} \cdot \hat{\boldsymbol{\sigma}} \cdot \boldsymbol{v} \, \mathrm{d}s, \tag{43}$$

where $\mathcal{S} = \mathcal{S}_0 + \mathcal{S}_\mathrm{w} + \mathcal{S}_\infty$ is the total surface bounding the flow, and $\mathcal{S}_\infty$ is the surface located at $\boldsymbol{r} \to \infty$. The latter does not contribute here. Using the boundary conditions for the model problem, we get:

$$\hat{\boldsymbol{V}} \cdot \boldsymbol{F} = -\hat{V} F_z = \int_{\mathcal{S}} \boldsymbol{n} \cdot \hat{\boldsymbol{\sigma}} \cdot \boldsymbol{v} \, \mathrm{d}s. \tag{44}$$

To find the force exerted on the sphere in the real problem, one needs to specify the boundary conditions for the real velocity field. Here, we assume that the sphere does not rotate, as in section , and we describe the flow in the translating reference frame of the particle. The no-slip boundary condition thus reads $\boldsymbol{v} = \boldsymbol{0}$ on $\mathcal{S}_0$. We further assume a small deformation of the wall, so that the velocity field at the undeformed wall surface can be obtained using the Taylor expansion:

$$\begin{aligned} \boldsymbol{v}|_{z=0} &= \boldsymbol{v}|_{z=\delta} - \delta \partial_z \boldsymbol{v}_0|_{z=0} \\ &= -u\boldsymbol{e}_x - \dot{d}\boldsymbol{e}_z + (\partial_t - u\partial_x)\delta \boldsymbol{e}_z - \delta \partial_z \boldsymbol{v}_0|_{z=0}, \end{aligned} \tag{45}$$

where $\boldsymbol{v}_0$ is the zeroth-order velocity field near a rigid surface. Using results from section , we find:

$$\partial_z \boldsymbol{v}_0|_{z=0} = -\frac{3\dot{d}r}{(d+\frac{r^2}{2a})^2}\boldsymbol{e}_r + \frac{2u}{5(d+\frac{r^2}{2a})}\left(\left(7 - \frac{6d}{d+\frac{r^2}{2a}}\right)\cos\theta \boldsymbol{e}_r - \sin\theta \boldsymbol{e}_\theta\right). \tag{46}$$

Combining Eqs. (42) and (44), we find the vertical force:

$$F_z = \frac{1}{\hat{V}} \int_{\mathbb{R}^2} \left(\hat{p}(-\dot{d} + \partial_t \delta - u\partial_x \delta) + \eta \partial_z \hat{\boldsymbol{v}}|_{z=0} \cdot \partial_z \boldsymbol{v}_0|_{z=0}\delta\right) \mathrm{d}\boldsymbol{r}. \tag{47}$$

After some algebra, and computing the integral in Fourier space, we recover the same expression as in Eq. (30), that reads:

$$F_z = -\frac{6\pi\eta a^2 \dot{d}}{d} + A\frac{\eta^2 u^2(\lambda+2\mu)}{\mu(\lambda+\mu)}\left(\frac{a}{d}\right)^{5/2} - B\frac{\eta^2 \dot{d}^2(\lambda+2\mu)}{\mu(\lambda+\mu)}\left(\frac{a}{d}\right)^{7/2} + C\frac{\eta^2 \ddot{d}a(\lambda+2\mu)}{\mu(\lambda+\mu)}\left(\frac{a}{d}\right)^{5/2}, \tag{48}$$

where the numerical coefficients A, B, C can be found analytically as:

$$A = \frac{9\pi}{25\sqrt{2}} \int_0^\infty k^2 K_0(k)\Big(-2K_1(k) + kK_2(k)\Big)\, k\mathrm{d}k = \frac{243\pi^3}{12800\sqrt{2}}, \tag{49}$$

$$B = 9\pi\sqrt{2} \int_0^\infty k^2 K_1(k)\left(K_2(k) - \frac{kK_3(k)}{8}\right) k\mathrm{d}k = \frac{3915\pi^3}{2048\sqrt{2}}, \tag{50}$$

$$C = \frac{9\sqrt{2}\pi}{2} \int_0^\infty k^2 K_1^2(k)\, \mathrm{d}k = \frac{27\pi^3}{32\sqrt{2}}, \tag{51}$$

and where K_i is the modified Bessel function of the second kind of order i [49].

Thin compressible substrate

In this appendix, we derive the EHD interactions exerted on a sphere immersed in a viscous fluid and near a thin compressible substrate of thickness h_sub. The deformation field follows the Winkler foundation:

$$\delta(\boldsymbol{r}, t) = -\frac{h_\mathrm{sub}}{(2\mu+\lambda)} p(\boldsymbol{r}, t), \tag{52}$$

which is valid for substrates of thickness smaller than the typical extent of the pressure field, namely the hydrodynamic radius $\sqrt{2ad}$ [20, 52, 56]. We perform the same asymptotic expansion as the one in section , defining the Winkler dimensionless compliance as [31]:

$$\kappa^{\mathrm{W}} = \frac{\sqrt{2}h_{\mathrm{sub}}\eta c a^{1/2}}{d^{*5/2}(2\mu+\lambda)}. \tag{53}$$

The leading-order substrate deformation, or equivalently here the leading-order pressure, reads:

$$H_1^{\mathrm{W}}(\boldsymbol{R},T) = P_0(\boldsymbol{R},T) = \frac{3\dot{D}}{2(D+R^2)^2} + \frac{6RU\cos\theta}{5(D+R^2)^2}. \tag{54}$$

The next-order pressure correction follows the same type of equation as in section :

$$\mathcal{L}.P_1^{\mathrm{W}} = F_0^{\mathrm{W}}(R,T) + F_1^{\mathrm{W}}(R,T)\cos\theta + F_2^{\mathrm{W}}(R,T)\cos 2\theta, \tag{55}$$

with:

$$F_0^{\mathrm{W}}(R,T) = -\frac{144R^2U^2}{25(D+R^2)^7}\left[D^2 - 6DR^2 + R^4\right] + \frac{18R^2\dot{D}^2}{(D+R^2)^7}\left[5D - 4R^2\right] - \frac{18R^2\ddot{D}}{(D+R^2)^5}, \tag{56}$$

and:

$$F_1^{\mathrm{W}}(R,T) = \frac{216R^3U\dot{D}}{5(D+R^2)^7}\left[-5D + R^2\right] + \frac{72R\dot{U}}{5(D+R^2)^5}. \tag{57}$$

We note that F_2^{W} does not contribute for the forces and torque, as in section . The isotropic component of the pressure can be found analytically, using polynomial fractions, as:

$$P_1^{\mathrm{W},(0)}(R,T) = \frac{9}{125}\frac{7-5Y^2}{(1+Y^2)^5}\frac{U^2}{D^4} - \frac{3}{40}\frac{71+55Y^2+30Y^4}{(1+Y^2)^5}\frac{\dot{D}^2}{D^5} + \frac{3}{2}\frac{1}{(1+Y^2)^3}\frac{\ddot{D}}{D^4}, \tag{58}$$

where $Y = R/D^{1/2}$ is the self-similar variable. However, the first angular component of the pressure does not exhibit such an analytical solution, and is thus found as in section by numerical integration of two scaling functions. Its general expression reads:

$$P_1^{\mathrm{W},(1)}(R,T) = \frac{U\dot{D}}{D^{9/2}}\phi^{\mathrm{W}}_{U\dot{D}}\left(\frac{R}{D^{1/2}}\right) + \frac{\dot{U}}{D^{7/2}}\phi^{\mathrm{W}}_{\dot{U}}\left(\frac{R}{D^{1/2}}\right). \tag{59}$$

Following the same calculation as in section , we find the vertical force as:

$$F_z^{\mathrm{W}} = -\frac{6\pi\eta a^2\dot{d}}{d} + \frac{48\pi}{125}\frac{\eta^2u^2h_{\mathrm{sub}}}{a(2\mu+\lambda)}\left(\frac{a}{d}\right)^3 - \frac{72\pi}{5}\frac{\eta^2\dot{d}^2h_{\mathrm{sub}}}{a(2\mu+\lambda)}\left(\frac{a}{d}\right)^4 + \frac{6\pi\eta^2\ddot{d}h_{\mathrm{sub}}}{(2\mu+\lambda)}\left(\frac{a}{d}\right)^3. \tag{60}$$

We stress that the prefactors $48\pi/125$ and 6π are in agreement with the results in [35] and [20], respectively. Similarly, the force along x reads:

$$F_x^{\mathrm{W}} = 6\pi\eta a u\left(\frac{8}{15}\log\left(\frac{d}{a}\right) - 0.95429\right) - 23.9\frac{\eta^2u\dot{d}h_{\mathrm{sub}}}{a(2\mu+\lambda)}\left(\frac{a}{d}\right)^3 + 4.520\frac{\eta^2\dot{u}h_{\mathrm{sub}}}{(2\mu+\lambda)}\left(\frac{a}{d}\right)^2. \tag{61}$$

The torque can be evaluated as well, and reads:

$$T_y^{\mathrm{W}} = 8\pi\eta u a^2\left(-\frac{1}{10}\log\left(\frac{d}{a}\right) - 0.19296\right) + 12.2\frac{\eta^2u\dot{d}h_{\mathrm{sub}}}{(2\mu+\lambda)}\left(\frac{a}{d}\right)^3 - 1.51\frac{\eta^2\dot{u}ah_{\mathrm{sub}}}{(2\mu+\lambda)}\left(\frac{a}{d}\right)^2. \tag{62}$$

All the prefactors for the EHD corrections of the lateral force and torque have been found numerically. Finally, following section , it is straightforward to generalize Eqs. (60), (61) and (62) in order to incorporate rotation.

Thin incompressible substrate

In this appendix, we suppose that the substrate of thickness h_{sub} is incompressible, *i.e.* of Poisson ratio $\nu = 1/2$, which means that the first Lamé coefficient λ is infinite. In this situation, the Winkler foundation is not valid. Instead, the mechanical response of a thin substrate follows the relation ([20, 56]):

$$\delta(\boldsymbol{r},t) = \frac{h_{\mathrm{sub}}^3}{3\mu}\boldsymbol{\nabla}^2 p(\boldsymbol{r},t), \tag{63}$$

where $\boldsymbol{\nabla}^2$ denotes the Laplacian operator. We perform the same asymptotic expansion as the one in section , defining the thin-incompressible dimensionless compliance as:

$$\kappa^{\text{t-i}} = \frac{\eta c h_{\mathrm{sub}}^3}{3\sqrt{2}\mu d^{*7/2} a^{1/2}}. \tag{64}$$

The leading-order substrate deformation reads:

$$H_1^{\text{t-i}}(\boldsymbol{R},T) = -\boldsymbol{\nabla}^2 P_0(\boldsymbol{R},T) = -\frac{12\dot{D}(D-2R^2)}{(D+R^2)^4} + \frac{48RU(2D-R^2)\cos\theta}{5(D+R^2)^4}. \tag{65}$$

The next-order pressure correction follows the same type of equation as in section :

$$\mathcal{L}.P_1^{\text{t-i}} = F_0^{\text{t-i}}(R,T) + F_1^{\text{t-i}}(R,T)\cos\theta + F_2^{\text{t-i}}(R,T)\cos 2\theta, \tag{66}$$

with:

$$\begin{aligned} F_0^{\text{t-i}}(R,T) = {} & \frac{1152R^2U^2\left(R^2-2D\right)\left(+2D^2-11R^2D+2R^4\right)}{25\left(D+R^2\right)^9} \\ & + \frac{432R^2\left(2D\left(D-5R^2\right)+3R^4\right)\dot{D}^2}{\left(D+R^2\right)^9} + \frac{144R^2\left(2R^2-D\right)\ddot{D}}{\left(D+R^2\right)^7}, \end{aligned} \tag{67}$$

and:

$$F_1^{\text{t-i}}(R,T) = -\frac{2592R^3\dot{D}U\left(7D^2-12R^2D+R^4\right)}{5\left(D+R^2\right)^9} - \frac{576R^3\dot{U}\left(-2D+R^2\right)}{5\left(D+R^2\right)^7}. \tag{68}$$

We note that $F_2^{\text{t-i}}$ does not contribute for the forces and torque, as in section . The isotropic component of the pressure can be found analytically, using polynomial fractions, as:

$$P_1^{\text{t-i},(0)}(R,T) = \frac{288\left(7Y^4-21Y^2+17\right)}{875\left(1+Y^2\right)^7}\frac{U^2}{D^5} + \frac{126Y^2-198}{7\left(1+Y^2\right)^7}\frac{\dot{D}^2}{D^6} + \frac{36}{5\left(1+Y^2\right)^5}\frac{\ddot{D}}{D^5}, \tag{69}$$

where $Y = R/D^{1/2}$ is the self-similar variable. However, the first angular component of the pressure does not exhibit such an analytical solution, and is thus found as in section by numerical integration of two scaling functions. Its general expression reads:

$$P_1^{\text{t-i},(1)}(R,T) = \frac{U\dot{D}}{D^{11/2}}\phi_{U\dot{D}}^{\text{t-i}}\left(\frac{R}{D^{1/2}}\right) + \frac{\dot{U}}{D^{9/2}}\phi_{\dot{U}}^{\text{t-i}}\left(\frac{R}{D^{1/2}}\right). \tag{70}$$

Following the same calculation as in section , we find the vertical force as:

$$F_z^{\text{t-i}} = -\frac{6\pi\eta a^2\dot{d}}{d} + \frac{432\pi}{875}\frac{\eta^2u^2h_{\mathrm{sub}}^3}{a^3\mu}\left(\frac{a}{d}\right)^4 - \frac{192\pi}{35}\frac{\eta^2\dot{d}^2h_{\mathrm{sub}}^3}{a^3\mu}\left(\frac{a}{d}\right)^5 + \frac{12\pi}{5}\frac{\eta^2\ddot{d}h_{\mathrm{sub}}^3}{a^2\mu}\left(\frac{a}{d}\right)^4. \tag{71}$$

We stress that the prefactor $12\pi/5$ is consistent with the linear-response theory in [20]. Similarly, the force along x reads:

$$F_x^{\text{t-i}} = 6\pi\eta a u\left(\frac{8}{15}\log\left(\frac{d}{a}\right) - 0.95429\right) - 12.2\frac{\eta^2 u\dot{d} h_{\text{sub}}^3}{a^3\mu}\left(\frac{a}{d}\right)^4 + 2.41\frac{\eta^2 \dot{u} h_{\text{sub}}^3}{a^2\mu}\left(\frac{a}{d}\right)^3. \tag{72}$$

The torque can be evaluated as well, and reads:

$$T_y^{\text{t-i}} = 8\pi\eta u a^2\left(-\frac{1}{10}\log\left(\frac{d}{a}\right) - 0.19296\right) + 7.75\frac{\eta^2 u\dot{d} h_{\text{sub}}^3}{a^2\mu}\left(\frac{a}{d}\right)^4 - 0.804\frac{\eta^2 \dot{u} h_{\text{sub}}^3}{a\mu}\left(\frac{a}{d}\right)^3. \tag{73}$$

* Electronic address: thomas.salez@u-bordeaux.fr

[1] D. Dowson and G. R. Higginson, Elasto-hydrodynamic lubrication: international series on materials science and technology (Elsevier, 2014).
[2] E. E. Brodsky and H. Kanamori, Journal of Geophysical Research: Solid Earth **106**, 16357 (2001).
[3] C. S. Campbell, The Journal of Geology **97**, 653 (1989).
[4] P. Karan, J. Chakraborty, and S. Chakraborty, Journal of the Indian Institute of Science **98**, 159 (2018).
[5] M. B. Jones, G. Fulford, C. P. Please, D. McElwain, and M. J. Collins, Bulletin of mathematical biology **70**, 323 (2008).
[6] V. C. Mow, M. H. Holmes, and W. M. Lai, Journal of biomechanics **17**, 377 (1984).
[7] S. Jahn, J. Seror, and J. Klein, Annual Review of Biomedical Engineering **18**, 235 (2016).
[8] J. P. Gong, Soft matter **2**, 544 (2006).
[9] K. Sekimoto and L. Leibler, EPL (Europhysics Letters) **23**, 113 (1993).
[10] N. Moyle, H. Wu, C. Khripin, F. Bremond, C.-Y. Hui, and A. Jagota, Soft matter **16**, 1627 (2020).
[11] H. Wu, N. Moyle, A. Jagota, and C.-Y. Hui, Soft Matter **16**, 2760 (2020).
[12] C.-Y. Hui, H. Wu, A. Jagota, and C. Khripin, Tribology Letters **69**, 1 (2021).
[13] R. H. Davis, J.-M. Serayssol, and E. Hinch, Journal of Fluid Mechanics **163**, 479 (1986).
[14] P. Gondret, M. Lance, and L. Petit, Physics of fluids **14**, 643 (2002).
[15] M. R. Tan, Y. Wang, and J. Frechette, Physical Review Fluids **4**, 084305 (2019).
[16] S. P. Meeker, R. T. Bonnecaze, and M. Cloitre, Physical Review Letters **92**, 198302 (2004).
[17] J. H. Snoeijer, J. Eggers, and C. H. Venner, Physics of Fluids **25**, 101705 (2013).
[18] D. Y. Chan, E. Klaseboer, and R. Manica, Soft Matter **5**, 2858 (2009).
[19] I. U. Vakarelski, R. Manica, X. Tang, S. J. O'Shea, G. W. Stevens, F. Grieser, R. R. Dagastine, and D. Y. Chan, Proceedings of the National Academy of Sciences **107**, 11177 (2010).
[20] S. Leroy and E. Charlaix, Journal of Fluid Mechanics **674**, 389 (2011).
[21] S. Leroy, A. Steinberger, C. Cottin-Bizonne, F. Restagno, L. Léger, and É. Charlaix, Physical Review Letters **108**, 264501 (2012).
[22] R. Villey, E. Martinot, C. Cottin-Bizonne, M. Phaner-Goutorbe, L. Léger, F. Restagno, and E. Charlaix, Physical Review Letters **111**, 215701 (2013).
[23] Y. Wang, C. Dhong, and J. Frechette, Physical Review Letters **115**, 248302 (2015).
[24] Y. Wang, G. A. Pilkington, C. Dhong, and J. Frechette, Current Opinion in Colloid & Interface Science **27**, 43 (2017).
[25] Y. Wang, M. R. Tan, and J. Frechette, Soft Matter **13**, 6718 (2017).
[26] D. Guan, E. Charlaix, R. Z. Qi, and P. Tong, Physical Review Applied **8**, 044010 (2017).
[27] Y. Wang, B. Zeng, H. T. Alem, Z. Zhang, E. Charlaix, and A. Maali, Langmuir **34**, 1371 (2018).
[28] A. Lainé, L. Jubin, L. Canale, L. Bocquet, A. Siria, S. H. Donaldson, and A. Niguès, Nanotechnology **30**, 195502 (2019).
[29] V. Bertin, Z. Zhang, R. Boisgard, C. Grauby-Heywang, E. Raphael, T. Salez, and A. Maali, ArXiv:2009.14531 (2020).
[30] J. Happel and H. Brenner, Low Reynolds number hydrodynamics: with special applications to particulate media, vol. 1 (Springer Science & Business Media, 2012).
[31] T. Salez and L. Mahadevan, Journal of Fluid Mechanics **779**, 181 (2015).
[32] J. Beaucourt, T. Biben, and C. Misbah, EPL (Europhysics Letters) **67**, 676 (2004).
[33] J. Skotheim and L. Mahadevan, Physical Review Letters **92**, 245509 (2004).
[34] J. Skotheim and L. Mahadevan, Physics of Fluids **17**, 092101 (2005).
[35] J. Urzay, S. G. Llewellyn Smith, and B. J. Glover, Physics of Fluids **19**, 103106 (2007).
[36] J. Urzay, Journal of fluid mechanics **653**, 391 (2010).
[37] X. Grandchamp, G. Coupier, A. Srivastav, C. Minetti, and T. Podgorski, Physical Review Letters **110**, 108101 (2013).
[38] M. Abkarian, C. Lartigue, and A. Viallat, Physical Review Letters **88**, 068103 (2002).
[39] A.-S. Bouchet, C. Cazeneuve, N. Baghdadli, G. S. Luengo, and C. Drummond, Macromolecules **48**, 2244 (2015).
[40] B. Saintyves, T. Jules, T. Salez, and L. Mahadevan, Proceedings of the National Academy of Sciences **113**, 5847 (2016), ISSN 0027-8424.
[41] H. S. Davies, D. Débarre, N. El Amri, C. Verdier, R. P. Richter, and L. Bureau, Physical Review Letters **120**, 198001 (2018).
[42] B. Rallabandi, N. Oppenheimer, M. Y. B. Zion, and H. A. Stone, Nature Physics **14**, 1211 (2018).
[43] P. Vialar, P. Merzeau, S. Giasson, and C. Drummond, Langmuir **35**, 15605 (2019).
[44] Z. Zhang, V. Bertin, M. Arshad, E. Raphael, T. Salez, and A. Maali, Physical Review Letters **124**, 054502 (2020).

[45] M. H. Essink, A. Pandey, S. Karpitschka, C. H. Venner, and J. H. Snoeijer, Journal of Fluid Mechanics **915** (2021).
[46] A. Pandey, S. Karpitschka, C. H. Venner, and J. H. Snoeijer, Journal of fluid mechanics **799**, 433 (2016).
[47] B. Rallabandi, B. Saintyves, T. Jules, T. Salez, C. Schonecker, L. Mahadevan, and H. A. Stone, Physical Review Fluids **2**, 074102 (2017).
[48] B. Saintyves, B. Rallabandi, T. Jules, J. Ault, T. Salez, C. Schonecker, H. A. Stone, and L. Mahadevan, Soft Matter **16**, 4000 (2020).
[49] M. Abramowitz and I. A. Stegun, Handbook of mathematical functions with formulas, graphs, and mathematical tables, vol. 55 (US Government printing office, 1964).
[50] A. Daddi-Moussa-Ider, B. Rallabandi, S. Gekle, and H. A. Stone, Physical Review Fluids **3**, 084101 (2018).
[51] H. Masoud and H. A. Stone, Journal of Fluid Mechanics **879** (2019).
[52] A. Kargar-Estahbanati and B. Rallabandi, Physical Review Fluids **6**, 034003 (2021).
[53] M. E. O'Neill, Mathematika **11**, 67 (1964).
[54] M. O'Neill and K. Stewartson, Journal of Fluid Mechanics **27**, 705 (1967).
[55] A. Goldman, R. Cox, and H. Brenner, Chemical engineering science **22**, 653 (1967).
[56] T. G. Chandler and D. Vella, Proceedings of the Royal Society A **476**, 20200551 (2020).